Available online at www.sciencedirect.com
ScienceDirect
Journal of Power Sources 181 (2008) 313–326
JOURNAL OF POWER SOURCES
www.elsevier.com/locate/jpowsour

Thermoeconomic modeling and parametric study of hybrid SOFC–gas turbine–steam turbine power plants ranging from 1.5 to 10 MWe

Alexandros Arsalis *

Department of Mechanical Engineering, Virginia Polytechnic Institute and State University, Blacksburg, VA 24061, USA

Received 24 September 2007; received in revised form 26 November 2007; accepted 30 November 2007
Available online 22 January 2008

Abstract

Detailed thermodynamic, kinetic, geometric, and cost models are developed, implemented, and validated for the synthesis/design and operational analysis of hybrid SOFC–gas turbine–steam turbine systems ranging in size from 1.5 to 10 MWe. The fuel cell model used in this research work is based on a tubular Siemens-Westinghouse-type SOFC, which is integrated with a gas turbine and a heat recovery steam generator (HRSG) integrated in turn with a steam turbine cycle. The current work considers the possible benefits of using the exhaust gases in a HRSG in order to produce steam which drives a steam turbine for additional power output. Four different steam turbine cycles are considered in this research work: a single-pressure, a dual-pressure, a triple pressure, and a triple pressure with reheat. The models have been developed to function both at design (full load) and off-design (partial load) conditions. In addition, different solid oxide fuel cell sizes are examined to assure a proper selection of SOFC size based on efficiency or cost. The thermoeconomic analysis includes cost functions developed specifically for the different system and component sizes (capacities) analyzed. A parametric study is used to determine the most viable system/component syntheses/designs based on maximizing total system efficiency or minimizing total system life cycle cost.

Keywords: Hybrid systems; SOFC; Gas turbine; Steam turbine; Cogeneration

1. Introduction

The combination of SOFCs with gas turbines is one of the most promising power generating applications [1,2]. The SOFC stack forms the combustor unit in a gas turbine system. Compressed air is fed into the SOFC stack where fuel is injected and electrical power drawn off. Operating close to a 46% conversion of fuel to electrical power [3], this SOFC then provides pressurized hot gases to a turbine operating at 35% electrical efficiency. The theoretical overall electrical conversion efficiency of this system can approach 65+%, which can be further improved by adding a steam turbine cycle to drive the overall electrical efficiency into the mid seventies [1,2].

The objective of this research work is to make a rigorous investigation of the design and performance characteristics of hybrid system configurations consisting of a SOFC, gas turbine, and steam turbine for stationary power applications which provide power to a large number of residential/commercial buildings. For example, a 10 MWe hybrid system can fulfill the needs of 2000 family residences based on an average four person family residence in the US which requires on average 5 kWe. To model and then analyze the hybrid system configurations as realistically as possible, detailed system/component thermodynamic, kinetic, geometric, and cost models are developed, implemented, validated and then used to conduct a parametric analysis of the key system/component parameters to investigate both thermodynamically (efficiency maximization) and economically (total life cycle cost minimization) the advantages that such hybrid systems might have over conventional GT–ST combined cycle systems, standalone SOFC systems, and hybrid SOFC–GT systems.

2. System layout

As a starting point for this research work, the modeling, computer code, and optimization results of a previously developed 1.5 MWe hybrid SOFC–GT plant Calise et al. [4–6] are used. In this work, the gas turbine exhaust mixture is re-circulated

* Tel.: +45 27282984; fax: +357 22 389423.
E-mail address: arsalis@vt.edu.

0378-7753/$ – see front matter © 2007 Elsevier B.V. All rights reserved.
doi:10.1016/j.jpowsour.2007.11.104

Nomenclature

A	heat transfer area (m^2)
D	diameter (m)
L	length (m)
$\dot{m}$	mass flow rate ($kg\,s^{-1}$)
n_{cell}	number of cells
$\dot{Q}$	heat transfer rate (kW)
T	temperature (K)
V	volume (m^3)
$\dot{W}$	power output (kW)

Subscripts

cell	SOFC stack
comp	compressor
cond	condenser
cool	cool water stream
gas	gas side stream
GT	gas turbine
HEC	counter-flow heat exchanger
i	inlet stream
o	outlet stream
PR	pre-reformer
pump	pump
ST	steam turbine
steam	steam side stream

and used to preheat the input air and fuel streams by means of heat exchangers, while the remaining energy is recovered to heat water for residential usage, while in the current work, this system has been modified and expanded to include a second bottoming cycle, utilizing various types (based on pressure level) of heat recovery steam generators and a steam turbine. In fact, four configurations are modeled and analyzed in detail here with the variations occurring with regard to the steam turbine (ST) bottoming cycle, i.e. a single-pressure level, a dual-pressure level, and a triple-pressure level with and without reheat. The purpose of using multiple-pressure levels is to achieve a higher power output from the steam turbine at the expense, of course, of extra equipment. The operation of the SOFC–GT topping cycle (see Fig. 1, top part) can be summarized as follows:

- Air is compressed by the air compressor (AC) up to the fuel cell operating pressure. The air is then brought to the cathode inlet of the SOFC stack (state point 18). Similarly, fuel is compressed by the fuel compressor (FC) and then brought to the anode compartment of the stack (state point 1).
- Both fuel and air can by-pass the fuel cell, i.e. a certain amount of fuel can flow directly to the combustor (C) by-passing the electrochemical reaction occurring within the stack (state point 23), while excess air can flow to the GT (state point 20).
- At the stack, fuel (state point 24) is mixed with the anode recirculation stream (state point 5) in order to support the steam reforming reaction in the pre-reformer and in the anode compartment of the fuel cell. The mixture at state point 25 consists of methane and steam. Thus, in the pre-reformer (PR), the first step in the fuel reforming process occurs. The energy required to support the pre-reforming reaction is derived from the hot stream at state point 26. The non-reacted fuel at state point 2 is involved in the internal reforming reaction within the anode compartment of the SOFC stack. Here, it is converted into the hydrogen that participates in the electrochemical reaction.
- On the cathode side, air is first preheated by a counter-flow heat exchanger air injection pipe (HEC) and then brought into the annulus (air pipe) of the SOFC where, at the three-phase boundaries, the cathode electrochemical reaction occur [1–2,7,8].
- The electrochemical reactions, occurring in the fuel cell, produce DC electrical current and release thermal energy. The first of these is converted into AC current by the inverter; the latter is used by the internal reforming reaction and to heat up the fuel cell stack.
- The high energy flow rate at state point 8 is first used to preheat air in the counter-flow heat exchanger and then to supply energy to the pre-reforming reaction. This stream at state point 21 enters the gas turbine.
- The expansion in the GT supplies mechanical power which in turn is converted into electric power.
- The operation of the steam turbine bottoming cycle, e.g., the triple pressure with reheat variation (see Fig. 1, bottom part), can be summarized as follows:
- The GT exhaust stream (state point 33) flows to the heat recovery steam generator (HRSG). The gas mixture side of the HRSG passes through the ten heat exchanger sections – high-pressure (HP) superheater (SU), reheater (RH), HP evaporator (EV), HP economizer (EC), intermediate-pressure (IP) SU, IP EV, IP EC, low-pressure (LP) SU, LP EV, and LP EC – and is exhausted at state point 34.
- The superheated steam produced by the HP SU (state point 35) is supplied to the HP stage of the steam turbine. After expansion the cold reheat (state point 64) at an intermediate pressure returns to the HRSG and there by means of a reheater is superheated (state point 66) and returned to the IP/LP steam turbine stage. Also the IP SU (state point 56) and the LP SU (state point 48) supply superheated steam to the double-admission IP/LP ST which during expansion produces mechanical power which in turn is converted into electric power in a generator. A small fraction of superheated steam at low pressure is extracted (state point 37) to the deaerator (DE) to be used later on for feedwater preheating.
- The wet steam (state point 38) is then condensed in the condenser (CON). The condensate (state point 39) enters the condensate pump (CP) and is then pumped to the DE at state point 40.
- In the DE, any air oddments and impurities contained by the water are removed while the water is preheated at 60 °C. The preheated water (state points 57, 49, 41) enters the HP FP (feedwater pump), IP FP, and LP FP, and is then pumped to the HP EC, IP EC and LP EC at state points 58, 50, and 42, respectively.

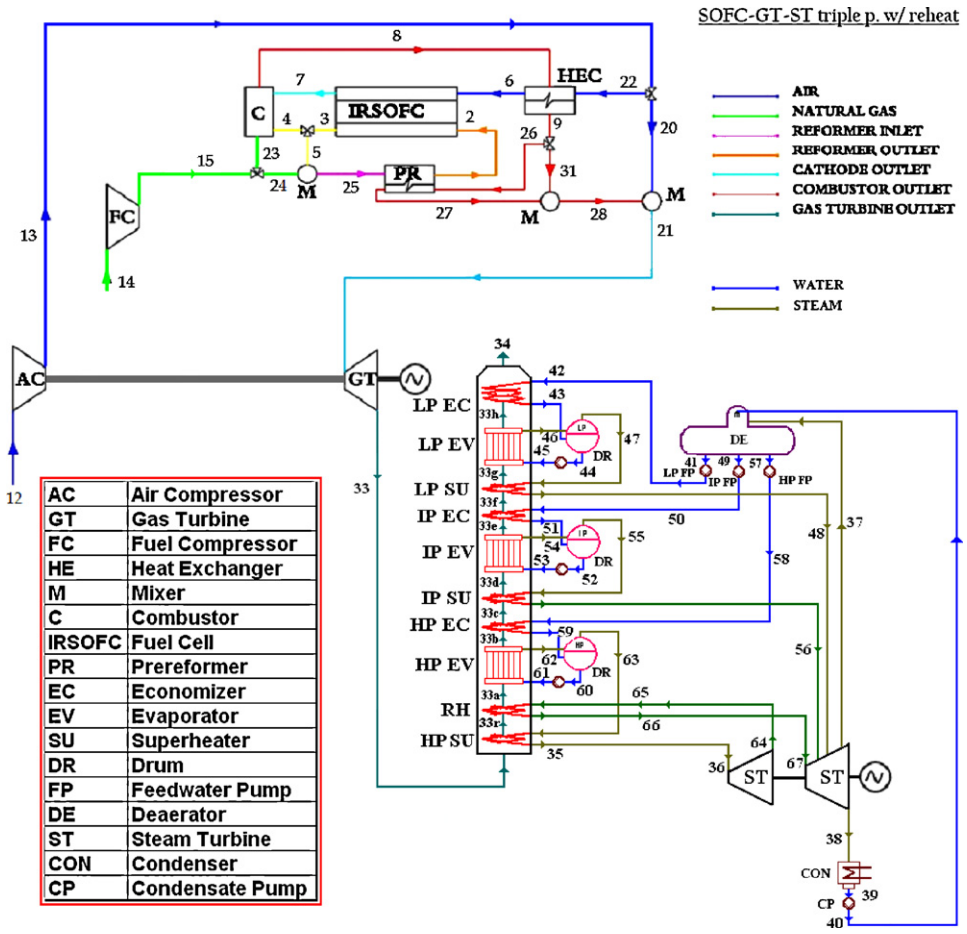

Fig. 1. SOFC–GT integrated with a triple pressure with reheat ST cycle.

- In the economizers, water is heated up to the saturated liquid point. Then it is evaporated at constant temperature/pressure in the evaporators.
- Water and saturated steam are separated in the drums, and the steam is supplied to the superheaters where it is superheated to the desired live steam temperatures and fed to the ST to repeat the cycle.

3. Plant model

The thermodynamic, geometric, kinetic and cost models were developed in MATLAB®. They are used to simulate the behavior of the hybrid fuel cell system configuration. The model is based on the following assumptions: one-dimensional flow; steady state; no gas leakage; negligible heat losses to the environment; negligible kinetic and gravitational terms in the energy balances.

3.1. Internal reforming SOFC model

The overall voltage of the single cell can be calculated as a function of current density, temperatures, pressures, chemical composition, and geometric/material characteristics by calculating the difference between the reversible potential and all the overvoltages [6], i.e.

$$V = E - V_{\text{act}} - V_{\text{ohm}} - V_{\text{conc}} \quad (1)$$

where V is the actual fuel cell potential, E the open circuit reversible voltage calculated on the basis of the Nernst equation, V_{act} the activation overvoltage calculated on the basis of the Butler-Volmer equation and experimental correlations for the anode and cathode exchange current densities, V_{ohm} the ohmic overvoltage, and V_{conc} the concentration overvoltage. Eq. (1) suggests that in the case of SOFCs, it is possible to neglect crossover, fuel, and internal current losses. The assumptions and calculation details for all aforementioned overvoltages are discussed more extensively in [6].

3.2. Pre-reformer model

One of the main advantages of using high temperature fuel cells is the possibility of feeding the SOFC with natural gas directly, since the reforming process can be supported inside the stack [1,7–10]. In practice, however, a pre-reforming process is usually necessary. The pre-reformer unit consists of a number of tubes located inside a shell and filled with a particular catalyst [11,12]. The reformate gas flows inside these tubes. Hot gases, coming from the combustor, flow inside the shell external to the tubes, supplying the thermal energy needed to support the process, since the energy provided by the exothermic water–gas shift reaction is not sufficient for the endothermic demethanization of the reforming process [11,12]. The pre-

reformer heat-exchange model is simulated taking into account both equilibrium and the kinetics as described in [6].

3.3. Gas turbine cycle model

The SOFC–GT subsystem utilizes an air compressor, fuel compressor, and gas turbine. The air compressor and gas turbine are connected together with a single shaft. The shaft is also connected to an electric generator converting the mechanical power to electrical power. Mass flow rates and rotor speeds are corrected on the basis of their inlet conditions according to [4–6,13,14].

3.4. Counter-flow heat exchanger air injection pipe, catalytic combustor, mixer, inverter, electric generator models

A counter-flow tube-in-tube heat exchanger is required in order to simulate the heat transfer in the air injection pipe between the air flowing through the fuel cell air tube and the stream coming from inside the stack [1–2,5–8,10,14–16]. The heat exchange is simulated on the basis of existing models in [5] and improved to include the effects of pressure drops and to take into account the dependence of the thermophysical and transport properties on temperature. The details of the counter-flow heat exchanger heat transfer model are given in [4].

The combustor burns any non-reacted fuel coming out of the fuel cell and, therefore, produces thermal energy for use elsewhere in the system. The hybrid plant makes use of three mixers. These are necessary for the operation and the regulation of the plant. The exerted electric signal needs to be conditioned before usage, converted to AC current, and filtered from possible oscillations. This is done by a DC–AC inverter. Similarly, the mechanical energy produced by the gas turbine must be converted to electric power. This conversion is accomplished by an electric generator.

3.5. Steam turbine cycle model

The main components of the steam turbine cycle include a steam turbine with an electric generator; a heat recovery steam generator which includes economizer(s), evaporator(s), superheater(s), and a reheater (triple-pressure reheat cycle only); a condenser which is dimensioned according to the turbine exit pressure and mass flow rate as well as ambient conditions; a deaerator heated by steam extracted from the steam turbine; a condensate pump; and one to three feedwater pumps.

The HRSG model calculates the live steam mass flow rates and also the exhaust gas conditions at the HRSG exit. In addition, it sizes the different types of heat exchangers included in the HRSG. Depending on the HRSG's number of pressure levels, the corresponding live steam mass flow rates are calculated. The water/steam conditions at the inlet and exit of every heat exchanger are defined either directly by the desired live steam conditions or indirectly through conditions on the saturation curve [17]. An important parameter defining the heating surface and performance of the HRSG is the pinch point. The pinch-point temperature is the difference between the evaporator's outlet temperature on the water/steam side and the inlet temperature on the exhaust gas side. The lower the pinch point, the more heating surface is required and the more steam is generated [18].

The desired live steam temperatures and pressures are fixed. The evaporator drum pressure can be determined based on a 7–10% loss from the live steam pressure. The pinch points are also selected and fixed. The energy balances on the gas and steam sides are:

$$\dot{Q}^{\text{gas}}_{\text{SU+EV}} = \dot{m}_{\text{GTexh}} c_{\text{p}} (T_{\text{SUin}} - T_{\text{EVout}}) \tag{2}$$

$$\dot{Q}^{\text{steam}}_{\text{SU+EV}} = \dot{m}_{\text{STin}} (h_{\text{SUout}} - h_{\text{EVin}}) \tag{3}$$

The heat transfer rate is determined from Eq. (2), and since the two heat transfer rates on the left hand side of each equation are equal to each other, Eq. (3) is solved for the live steam mass flow rate. Using simple energy balances, identical to the preceding ones, all temperatures and heat transfer rates can be calculated for all the heat exchangers.

For the geometric models of the heat exchangers, both the LMTD and effectiveness-NTU methods are used depending on the exchanger. The geometric models are needed for determining off-design behavior. All the heat exchangers are shell-and-tube since they are the appropriate type for compact heat recovery steam generators [19]. The necessary equations for shell-and-tube heat exchangers are obtained from [19]. A detailed analysis of all the heat exchangers' geometric models can be found in [20].

The axial-flow steam turbine can be single, dual, or triple admission depending on the HRSG's pressure level. Furthermore, in the triple-pressure reheat cycle configuration, it is divided into two sections: a high pressure (HP) section and an intermediate/low-pressure (IP/LP) section. In this particular configuration, the HP section is supplied with live steam from the superheater. After expansion, the steam returns to the reheater in the HRSG where it is superheated and supplied to the IP/LP section for further expansion. Following expansion, the exhaust is fed to the condenser. All the configurations include extraction outlets for deaerating/preheating. The mass and energy balances for the triple-pressure reheat cycle are

$$\dot{m}^{\text{ST}}_{\text{HP}_{\text{in}}} + \dot{m}^{\text{ST}}_{\text{RH}_{\text{in}}} + \dot{m}^{\text{ST}}_{\text{IP}_{\text{in}}} + \dot{m}^{\text{ST}}_{\text{LP}_{\text{in}}} = \dot{m}^{\text{ST}}_{\text{RH}_{\text{out}}} + \dot{m}^{\text{ST}}_{\text{ext}} + \dot{m}^{\text{ST}}_{\text{out}} \tag{4}$$

$$\begin{aligned}\dot{W}^{\text{triple RH}}_{\text{ST}} = {} & \dot{m}^{\text{ST}}_{\text{HP}_{\text{in}}} h^{\text{ST}}_{\text{HP}_{\text{in}}} + \dot{m}^{\text{ST}}_{\text{RH}_{\text{in}}} h^{\text{ST}}_{\text{RH}_{\text{in}}} + \dot{m}^{\text{ST}}_{\text{IP}_{\text{in}}} h^{\text{ST}}_{\text{IP}_{\text{in}}} + \dot{m}^{\text{ST}}_{\text{LP}_{\text{in}}} h^{\text{ST}}_{\text{LP}_{\text{in}}} \\ & - \dot{m}^{\text{ST}}_{\text{RH}_{\text{out}}} h^{\text{ST}}_{\text{RH}_{\text{out}}} - \dot{m}^{\text{ST}}_{\text{ext}} h^{\text{ST}}_{\text{ext}} - \dot{m}^{\text{ST}}_{\text{out}} h^{\text{ST}}_{\text{out}}\end{aligned} \tag{5}$$

where $\dot{m}^{\text{ST}}_{\text{HP}_{\text{in}}}$, $\dot{m}^{\text{ST}}_{\text{RH}_{\text{in}}}$, $\dot{m}^{\text{ST}}_{\text{IP}_{\text{in}}}$, and $\dot{m}^{\text{ST}}_{\text{LP}_{\text{in}}}$ are the mass flow rates of the HP, RH, IP, and LP superheated steam entering the steam turbine, respectively, and $\dot{m}^{\text{ST}}_{\text{RH}_{\text{out}}}$ the mass flow rate of the steam after expansion in the HP section of the steam turbine. For off-design purposes steam turbine maps are used in order to capture the effects of geometry on turbine performance. To generate these maps for different size turbines, data is taken from [21].

The steam turbine cycle includes a condensate pump and one to three feedwater pumps depending on the number of HRSG pressure levels. Since the thermodynamic states in the inlet are known and the outlet thermodynamic states can be fixed as desired, what is left is a calculation of the pump power consumed. The corresponding mass and energy balances are given by

$$\dot{m}_{\text{in}}^{\text{pump}} = \dot{m}_{\text{out}}^{\text{pump}} \tag{6}$$

$$\dot{W}_{\text{pump}} = [\dot{m}_{\text{in}}(h_{\text{out}} - h_{\text{in}})]_{\text{pump}} \tag{7}$$

where $\dot{m}_{\text{in}}$ is the non-pressurized mass flow rate entering the pump, $\dot{m}_{\text{out}}$ the pressurized mass flow rate exiting the pump, $\dot{W}_{\text{pump}}$ the pump work rate consumption, and $h_{\text{in}}^{\text{pump}}$ and $h_{\text{out}}^{\text{pump}}$ are the corresponding enthalpies for the mass flow. Again, for off-design purposes, pump maps are rescaled and modified from actual pump maps found in the literature. For the condensate pump, a map from [22] for a centrifugal type pump is used while for the feedwater pumps, a map for a displacement type pump from [23] is employed.

The condenser, which is a shell-and-tube heat exchanger, receives wet steam from the steam turbine's exhaust and condenses it to a saturated liquid. In the condensing process, the temperature and pressure are kept constant. For the purposes of this study, they have been fixed at 31 °C and 0.045 bar as in [18]. The working side mass balance is:

$$\dot{m}_{\text{in}}^{\text{cond}} = \dot{m}_{\text{out}}^{\text{cond}} \tag{8}$$

where $\dot{m}_{\text{in}}^{\text{cond}}$ is the mass flow rate of the wet steam entering the condenser and $\dot{m}_{\text{out}}^{\text{cond}}$ the mass flow rate of the saturated liquid exiting. The heat rejected to the cooling water is found from an energy balance on the condensing steam, i.e.

$$\dot{Q}_{\text{cond}} = [\dot{m}_{\text{in}}^{\text{cond}}(h_{\text{in}}^{\text{cond}} - h_{\text{out}}^{\text{cond}})] \tag{9}$$

where $\dot{Q}_{\text{cond}}$ is the rejected heat transfer rate and $h_{\text{in}}^{\text{cond}}$, $h_{\text{out}}^{\text{cond}}$ are the enthalpies for the corresponding mass flow rates. The cooling water mass flow rate can be calculated by an energy balance on the cooling water entering and exiting the condenser:

$$\dot{m}_{\text{cw}} = \frac{\dot{Q}_{\text{cond}}}{(T_{\text{cw,out}} - T_{\text{cw,in}})C_{\text{pcw}}} \tag{10}$$

where $\dot{m}_{\text{cw}}$ is the mass flow rate of the cooling water, $T_{\text{cw,in}}$ and $T_{\text{cw,out}}$ are the inlet and outlet cooling water temperatures, respectively, and $C_{\text{p,cw}}$ is the average cooling water specific heat. The LMTD method is applied to the geometric analysis of the condenser analyzed in detail in [20].

The deaerator removes dissolved gases and impurities from the condensate by keeping it in a reservoir at the state of a saturated liquid absorbing heat extracted from the steam turbine at a pressure slightly higher than the deaerator pressure. The corresponding mass and energy balances are

$$\dot{m}_{\text{in}}^{\text{dea}} + \dot{m}_{\text{ext}}^{\text{dea}} = \dot{m}_{\text{out}}^{\text{dea}} \tag{11}$$

where $\dot{m}_{\text{in}}^{\text{dea}}$ is the mass flow rate of the saturated liquid coming from the condensate pump, $\dot{m}_{\text{ext}}^{\text{dea}}$ the mass flow rate of the steam turbine extraction, $\dot{m}_{\text{out}}^{\text{dea}}$ the mass flow rate of the deaerated/preheated water exiting the deaerator. An energy balance on this component yields

$$\dot{m}_{\text{out}}^{\text{dea}} h_{\text{out}}^{\text{dea}} - \dot{m}_{\text{ext}}^{\text{dea}} h_{\text{ext}}^{\text{dea}} - \dot{m}_{\text{in}}^{\text{dea}} h_{\text{in}}^{\text{dea}} = 0 \tag{12}$$

where $h_{\text{out}}^{\text{dea}}$, $h_{\text{ext}}^{\text{dea}}$, and $h_{\text{in}}^{\text{dea}}$ are the enthalpies for the corresponding mass flow rates.

4. Cost model

For the thermoeconomic analysis of the plant, appropriate cost functions must be formulated to include the purchase cost for every component, the capital cost per annum, the operating cost per annum, and the total cost per annum. The expressions for all the component purchase costs are summarized in detail in Table 1, while those for the capital, operating, and total costs per annum are summarized in Table 2.

For the gas turbine, the cost function proposed by [24] is used. For the centrifugal compressors (air and fuel compressors), the corresponding costs are calculated by interpolating data from the manufacturers as a function of the maximum power required and using information provided by [25]. For the counter-flow heat exchanger, the capital cost is determined on the basis of a cost function from [26] while the cost of the SOFC stack is estimated with reference to market studies in which the expected cost for the case of a significant increase in production volume is assumed. A detailed work performed by [9] relates the SOFC purchase cost to the active area and the operating temperature. Furthermore, the electric energy produced by the SOFC must be filtered by an inverter, whose cost is not negligible and should, therefore, be taken into account [9]. The SOFC system also consists of a pre-reformer, whose cost is calculated on the basis of its catalysts volume and the finned exchange area [11–12,26] which in turn is related to the number, diameter, and length of tubes. Thus, based on these references and updating the functions with literature data, the pre-reformer component cost function is formulated by [4]. The total cost for SOFC auxiliary devices such as the combustor, mixers, and by-pass valves are calculated as a fixed percentage (10%) of the stack cost.

For the steam turbine cycle, all cost equations, except that for the steam turbine, are based on [17] and have been appropriately adjusted for inflation by using [27]. For the steam turbine, the cost function, which is based on the steam turbine power output, is developed based on [28]. For the HRSG (which includes the drum and piping costs), the total cost is composed of the cost for the various heat exchangers, the piping, the gas conduit, and the pump. It is based on a function used by [29]. The total cost of the heat exchangers is formed by the sum of the cost for the various heat exchange units (e.g., HP superheater, HP evaporator, HP economizer, reheater, etc.) indicated by the index i. Also the LMTD correction factor, K_i is based on the logarithmic mean temperature difference, $\Delta T_{\text{lm},i}$, while f_{p_i}, $f_{T_{i,\text{steam}}}$, and $f_{T_{i,\text{gas}}}$ are cost correction factors. The cost functions for the piping and the gas conduit include the factors f_{p_i}, $f_{T_{i,\text{steam}}}$, and $f_{T_{i,\text{gas}}}$. The factors introduce a sensitivity of cost to pressure as well as to steam and exhaust gas temperature. The pressure factor is

Table 1
Component cost models

	Variable description	Model equation
C_{GT}	Gas turbine component cost ($)	$C_{GT} = (-98.328\ \ln(\dot{W}_{GT}) + 1318.5)\dot{W}_{GT}$
C_{comp}	Compressor component cost ($)	$C_{comp} = 91562(\dot{W}_{comp}/445)^{0.67}$
C_{HEC}	Counter-flow heat exchanger component cost ($)	$C_{HEC} = 130(A_{HEC}/0.093)^{0.78}$
C_{SOFC}	SOFC stack component cost ($)	$C_{SOFC} = (n_{cells}\pi D_{cell}L_{cell})(2.96T_{cell} - 1907)$
C_{inv}	Inverter component cost ($)	$C_{inv} = 10^5(\dot{W}_{cell}/500)^{0.70}$
C_{PR}	Pre-reformer component cost ($)	$C_{PR} = 130(A_{PR,fin}/0.093)^{0.78} + 3240(V_{PR})^{0.4} + 21{,}280.5V_{PR}$
$C_{aux,SOFC}$	SOFC auxiliary components cost ($)	$C_{aux,SOFC} = 0.10C_{SOFC}$
C_{ST}	Steam turbine component cost ($)	$C_{ST} = 3644.3(\dot{W}_{ST})^{0.7} - 61.3(\dot{W}_{ST})^{0.95}$
f_{p_i}	Heat exchanger pressure factor	$f_{p_i} = 0.0971(p_i/30) + 0.9029$
$f_{T,steam}$	Steam-side temperature factor	$f_{T,steam} = 1 + \exp(T_{out,steam} - 830/500)$
$f_{T,gas}$	Gas-side temperature factor	$f_{T,gas} = 1 + \exp(T_{out,gas} - 990/500)$
K_i	LMTD correction factor (kW K^{-1})	$K_i = (\dot{Q}_i/\Delta T_{lm,i})$
$C_{HE(HRSG)}$	HRSG's heat exchangers component cost ($)	$C_{HE(HRSG)} = 3650\sum_i (f_{p_i} f_{T_{i,steam}} f_{T_{i,gas}} K^{0.8})_i$
f_{p_j}	Piping pressure factor	$f_{p_j} = 0.0971(p_j/30) + 0.9029$
C_{piping}	HRSG's piping component cost ($)	$C_{piping} = 11,820\sum_j (f_{p_j}\dot{m}_{j,steam})$
C_{gas}	HRSG's gas conduit cost ($)	$C_{gas} = 658\dot{m}_{gas}^{1.2}$
C_{HRSG}	HRSG component cost ($)	$C_{HRSG} = C_{HE(HRSG)} + C_{piping} + C_{gas}$
C_{cond}	Condenser component cost ($)	$C_{cond} = 248A_{cond} + 659\dot{m}_{cool}$
f_η	Efficiency correction factor	$F_\eta = 1 + (1 - 0.8/1 - \eta_{pump})$
C_{pump}	Pump component cost ($)	$C_{pump} = 442(\dot{W}_{pump})^{0.71}1.41f_\eta$

calculated as a function of live steam pressure P_i and comes from curve fit data for heat exchangers found in [26]. The temperature factors are developed using the [29] form of the temperature correction factors and the fact that the investment of superheaters is about twice as high as the investment cost for evaporators [17]. The temperature values indicating technical limits are taken from [17].

For the condenser, the cost function is based on [29]. It is calculated as a function of the condenser surface area, A_{cond}, and the cooling water mass flow rate, $\dot{m}_{cool}$. For the deaerator, the cost function is formulated using a cost function found in [26]. The cost function for the pumps is taken from [29] and calculates the cost as a function of the electric power consumed, $\dot{W}_{pump}$, and an efficiency correction factor f_η.

The capital cost must be placed on an annual basis in order to account for the cost of the investment required. This annual cost is composed of the depreciation cost, $\dot{C}_{dep}$, interest on the investment, $\dot{C}_{int}$, maintenance cost, $\dot{C}_{mai}$, insurance cost, $\dot{C}_{ins}$, and tax cost, $\dot{C}_{tax}$. The depreciation cost is based on the fact that the equipment deteriorates with time [30] and, thus, looses value. This loss of value needs to be distributed over the lifetime of the component. This results in a realistic estimation of the cost of the equipment and indicates how much money has to be spent every year in order to save money for future replacement or to pay back loans if the equipment was purchased with outside capital. In the context of thermoeconomic modeling, the common linear depreciation method is used for this cost estimation. Therefore, the annual depreciation cost is determined by dividing the total purchase cost, C_{pur}, by the depreciation time, n_{dep}, measured in years. For this research work, n_{dep} has been assumed to be 10 years [4].

The purchase or capital cost must also be financed from outside sources such as bank loans. The associated interest is considered a cost [30]. For the current research work, some simplifying assumptions are made: (i) a single interest rate is assumed for the cost of borrowed capital as well as for the opportunity cost of having invested ones own capital and (ii) the capital cost is distributed over the lifetime or depreciation time of the plant. The interest rate, i, is assumed to be 0.0926 [30].

Table 2
Capital, operating, and total cost models

	Variable description	Model equation
$\dot{C}_{dep}$	Depreciation cost ($ year^{-1})	$\dot{C}_{dep} = C_{pur}/n_{dep}$, $\dot{C}_{int} = (C_{pur}/n_{dep})i$,
$\dot{C}_{int}$	Interest on outside capital cost ($ year^{-1})	$\dot{C}_{mai} = (C_{pur}/n_{dep})f_{mai}$
$\dot{C}_{mai}$	Maintenance cost ($ year^{-1})	
$\dot{C}_{ins}$	Insurance cost ($ year^{-1})	$\dot{C}_{ins} = (C_{pur}/n_{dep})f_{ins}$,
$\dot{C}_{tax}$	Taxation cost ($ year^{-1})	$\dot{C}_{tax} = (C_{pur}/n_{dep})f_{tax}$
$\dot{C}_{cap}$	Capital cost ($ year^{-1})	$\dot{C}_{cap} = \dot{C}_{dep} + \dot{C}_{int} + \dot{C}_{mai} + \dot{C}_{ins} + \dot{C}_{tax}$, $\dot{C}_{ope} = c_f\dot{V}_f N_h$
$\dot{C}_{ope}$	Operating cost ($ year^{-1})	$\dot{C}_{total} = \dot{C}_{cap} + \dot{C}_{ope}$
$\dot{C}_{total}$	Total cost ($ year^{-1})	

The maintenance cost may vary over the lifetime of an installation as the equipment degrades and depends largely on the number of operating hours, the frequency of shutdowns and startups, and the operating environment. A total maintenance cost for the above suggests annual maintenance expenses on the order of 6% of the annual depreciation cost [11]. Thus, f_{mai} which is the maintenance cost factor is 0.06. Similarly, the insurance and taxation cost factors are chosen as 0.2 and 0.54%, respectively [17].

The operating cost per annum is based on [4]. In this cost function, c_f is the cost of fuel in $\$\,Nm^{-3}$, $\dot{V}_f$ is the volumetric flow rate of the fuel in $Nm^3\,h^{-1}$, and N_h are the annual hours of operation. The latter is assumed to be $8760\,h\,year^{-1}$ [4]. Once both the annual operating cost and the capital cost per annum are known, the total cost per annum becomes the sum of the annual capital and operating costs.

5. Model validation

The SOFC–GT–ST hybrid system needs to be validated in order to have confidence in the model predictions. The validation procedure helps determine the degree of accuracy of the model and any possible mismatches and discrepancies. Each subsystem of the hybrid system is validated separately using manufacturer's data for the SOFC model [4–6] and measured data from the literature for the steam turbine cycle models.

As mentioned previously, the steam turbine cycle subsystem models were modeled based on [18]. Fortunately, the same source includes measured data for the performance of all four steam turbine cycle configurations. This data includes temperatures, pressures, mass flow rates, and steam turbine power output. Detailed comparisons of these data can be found in [20]. The comparison indicates good agreement between the measured values from the literature and those calculated from the models. The few configurational differences which do exist are justified by the differences which exist between the cycles found in the literature and the model configurations used here. These differences include the following: simplification of the HRSG's heat exchangers from dual flow to single flow, a different chemical composition for the GT exhaust gases, a pressure loss (2%) for every heat exchanger in the HRSG for all model calculations different from that in [18], and a model pump power expenditure calculation somewhat different than that found in [18]. The slightly lower live steam production, and in effect the slightly lower ST power output for all model configurations as compared with [18], is mainly caused by the absence of a GT cooler.

A second validation was also made to check in more detail the steam production using results more suitable to fuel cell hybrid systems. These results are from a simple, single-pressure HRSG. These were found in [2]. The model and literature results comparison can be found in [20]. The minor differences between the literature and the model results are caused by the assumptions of a constant specific heat throughout the HRSG in the literature results as well as of no heat exchanger pressure losses in the literature results.

6. Parametric study: results and discussion

The purpose of the parametric study is to either maximize the average efficiency or minimize the total cost of the hybrid SOFC–GT–ST power plant. To achieve this, a systematic variation in the values of a number of key decision variables as well as the relative sizes of the SOFC, GT, and ST for a given hybrid plant size must be made. The key decision variable ranges and initial values are chosen on the basis of typical hybrid fuel cell systems found in [4–6]. The fuel utilization factor is varied from 0.75 to 0.90 in 0.05 increments. Values below 0.75 are not applicable because such values cause an increase in temperature beyond the maximum possible turbine inlet temperature (TIT) and, therefore, a coupling point of the air compressor and the gas turbine cannot be reached. In addition, lower fuel utilization factors result in lower efficiencies since fuel is converted mainly in the combustor.

The steam-to-carbon ratio is varied from 2 to 3.5 in 0.5 increments. Values below 2 are not included in order to avoid problems of carbon deposition on the anode of the SOFC stack as reported in [1–2,8].

The SOFC operating temperature is varied from 950 to 1100 °C in 50 °C increments. A value beyond 1100 is not used because it would exceed the operating limit of the SOFC. Also, a value lower than 950 °C at full load (i.e. at the design point) is infeasible since the minimum part load (25%) SOFC operating temperature is not high enough to heat the SOFC stack.

The SOFC operating pressure is varied from 7 to 10 bar in 1 bar increments. A value beyond 10 bar is not used because the differential pressure between the anode and the cathode compartments of the SOFC would exceed the operating limits set by the simulation process as described in [6].

Finally, the unit cost of fuel is varied as follows: 0.1, 0.3, 0.6, 0.9, and 1.2. The initial value of 0.3 is the one published in [31] for the year 2005.

Three different hybrid plant sizes are considered: 1.5, 5, and 10 Mwe, where two different SOFC sizes are considered based on current density. The operating current density for the selected fuel cell operates from 100 to 650 $mA\,cm^{-2}$ [32]. Since the current density decreases at off-design, the small SOFC is selected based on a maximum possible current density of 550 $mA\,cm^{-2}$ (full load or design condition) while the large SOFC is selected based on a minimum possible current density of 100 $mA\,cm^{-2}$ (25% full load condition). The larger SOFC yields higher efficiencies as compared with the smaller SOFC but the latter has a lower capital cost which is significant since the SOFC purchase cost is the most dominant of all the equipment purchase costs. In the parametric study conducted here, the smaller SOFC minimizes the total cost while the larger one maximizes the efficiency. Also, the gas turbine and steam turbine sizing is determined based on the extra power needed to reach the desired total power output.

The performance of each individual system is analyzed at full and part load conditions to determine the average and total efficiencies and total operating cost. The load profile is based on a 2-day (one average winter day and one average summer day), electrical power demand profile for an average four person

family household [33] scaled appropriately to coincide with the three different sized hybrid plants analyzed here and extended over an entire year. The average efficiency for the plant becomes a time-averaged value based on the time intervals. It is defined as follows:

$$\eta_{\text{ave}} = \frac{\Delta t_1 \eta_1 + \Delta t_2 \eta_2 + \Delta t_3 \eta_3 + \Delta t_4 \eta_4}{\sum \Delta t_i} \tag{13}$$

where the Δt_1, Δt_2, Δt_3, and Δt_4 are the time intervals corresponding to 25, 50, 75, and 100% loads (values shown in Table 3), and the η_1, η_2, η_3, and η_4 are the hybrid plant energetic electrical efficiencies corresponding to the above time intervals.

Table 3
Time intervals for Eq. (13)

Variable description	Value (days)	Variable description	Value (days)
Δt_1 25% load	137	Δt_3 75% load	106
Δt_2 50% load	46	Δt_4 100% load	76

In addition, the total efficiency is defined as

$$\eta_{\text{tot}} = \frac{\sum \dot{W}_i \, \Delta t_i}{\sum \dot{Q}_{\text{H}} \, \Delta t_i} \tag{14}$$

where $\dot{W}_i$ is the power output corresponding to 25, 50, 75, and 100% load, and $\dot{Q}_{\text{H}}$ the heat input to the system based

Table 4
Parametric results for the 10 MWe triple-pressure w/RH ST hybrid system

Decision variables					Objective functions			Power output (MW)		
U_{f}	T_{SOFC}	S/C	p_{SOFC}	c_{fuel}	η_{ave}	C_{total}	η_{tot}	$\dot{W}_{\text{SOFC}}$	$\dot{W}_{\text{GT}}$	$\dot{W}_{\text{ST}}$
Hybrid system employed with a small SOFC										
0.75	1000	2	8	0.3	0.5864	3,846,790	0.6240	7.863	2.308	1.337
0.8	1000	2	8	0.3	0.5852	3,852,258	0.6213	7.902	2.356	1.398
0.85	1000	2	8	0.3	0.5889	3,637,267	0.6242	7.958	2.400	1.454
0.9	1000	2	8	0.3	0.5685	3,741,024	0.6039	8.001	2.447	1.510
0.85	950	2	8	0.3	0.5665	3,690,959	0.6030	7.999	2.439	1.407
0.85	1000	2	8	0.3	0.5889	3,637,267	0.6242	7.958	2.400	1.454
0.85	1050	2	8	0.3	0.5960	3,660,018	0.6300	7.902	2.358	1.506
0.85	1100	2	8	0.3	0.6032	3,692,544	0.6368	7.856	2.310	1.548
0.85	1000	2	8	0.3	0.5889	3,637,267	0.6242	7.958	2.400	1.454
0.85	1000	2.5	8	0.3	0.5822	3,653,267	0.6178	8.006	2.447	1.405
0.85	1000	3	8	0.3	0.5810	3,644,914	0.6166	8.059	2.489	1.360
0.85	1000	3.5	8	0.3	0.5716	3,689,910	0.6079	8.102	2.537	1.307
0.85	1000	2	7	0.3	0.5848	3,645,623	0.6192	7.906	2.354	1.403
0.85	1000	2	8	0.3	0.5889	3,637,267	0.6242	7.958	2.400	1.454
0.85	1000	2	9	0.3	0.5869	3,641,883	0.6214	8.001	2.441	1.498
0.85	1000	2	10	0.3	0.5852	3,648,621	0.6197	8.054	2.496	1.543
0.85	1000	2	8	0.1	0.5889	1,744,829	0.6242	7.958	2.400	1.454
0.85	1000	2	8	0.3	0.5889	3,637,267	0.6242	7.958	2.400	1.454
0.85	1000	2	8	0.6	0.5889	6,415,426	0.6242	7.958	2.400	1.454
0.85	1000	2	8	0.9	0.5889	9,217,784	0.6242	7.958	2.400	1.454
0.85	1000	2	8	1.2	0.5889	12,032,142	0.6242	7.958	2.400	1.454
Hybrid system employed with a large SOFC										
0.75	1000	2	8	0.3	0.6298	3,798,306	0.6616	8.303	2.154	1.187
0.8	1000	2	8	0.3	0.6367	3,756,709	0.6659	8.347	2.203	1.126
0.85	1000	2	8	0.3	0.6529	3,697,652	0.6836	8.391	2.254	1.079
0.9	1000	2	8	0.3	0.6304	3,781,486	0.6605	8.442	2.304	1.005
0.85	950	2	8	0.3	0.6447	3,625,057	0.6741	8.440	2.997	1.007
0.85	1000	2	8	0.3	0.6529	3,697,652	0.6836	8.391	2.254	1.079
0.85	1050	2	8	0.3	0.6412	3,834,151	0.6707	8.344	2.201	1.130
0.85	1100	2	8	0.3	0.6386	3,926,399	0.6677	8.301	2.149	1.189
0.85	1000	2	8	0.3	0.6529	3,697,652	0.6836	8.391	2.254	1.079
0.85	1000	2.5	8	0.3	0.6433	3,737,498	0.6722	8.442	2.305	1.011
0.85	1000	3	8	0.3	0.6357	3,748,615	0.6657	8.496	2.347	0.952
0.85	1000	3.5	8	0.3	0.6337	3,774,777	0.6641	8.534	2.396	0.894
0.85	1000	2	7	0.3	0.6368	3,823,306	0.6658	8.346	2.203	1.008
0.85	1000	2	8	0.3	0.6529	3,697,652	0.6836	8.391	2.254	1.079
0.85	1000	2	9	0.3	0.6348	3,840,558	0.6644	8.435	2.301	1.136
0.85	1000	2	10	0.3	0.6316	3,871,101	0.6610	8.493	2.348	1.189
0.85	1000	2	8	0.1	0.6529	1,985,021	0.6836	8.391	2.254	1.079
0.85	1000	2	8	0.3	0.6529	3,697,652	0.6836	8.391	2.254	1.079
0.85	1000	2	8	0.6	0.6529	6,281,601	0.6836	8.391	2.254	1.079
0.85	1000	2	8	0.9	0.6529	8,859,549	0.6836	8.391	2.254	1.079
0.85	1000	2	8	1.2	0.6529	11,449,497	0.6836	8.391	2.254	1.079

on the LHV and fuel flow rates for the aforementioned time intervals.

Results for all the hybrid systems modeled and simulated here are analyzed thoroughly in [20]. A representative set of results for the parametric study performed for the 10 MWe SOFC–GT–ST hybrid system with a triple pressure with reheat ST cycle is shown in Table 4 and Figs. 2 and 3. The top half of Table 4 shows the results for the small SOFC, while the bottom half shows those for the large SOFC. The objective function is the average efficiency when using a large SOFC and the total cycle cost for the small SOFC. Figs. 2 and 3 show the decision variable values plotted against the corresponding objective function values.

From an observation of the trend lines shown in these figures, some general remarks can be made that apply to all the hybrid plants analyzed here. The optimum fuel utilization factor (U_f) is 0.85. For the small SOFC where the cost is the optimizing function of interest, the minimum total cost is achieved at this value because although the capital cost decreases slightly at lower values of U_f, the more dominating operating cost is decreased at higher values of U_f. Therefore, the higher efficiency is the main reason that the higher fuel utilization is more economical even though only slightly so.

For the large SOFC, where the average efficiency is the optimizing function of interest, as expected, the higher the fuel utilization factor is the higher the efficiency. The optimum value

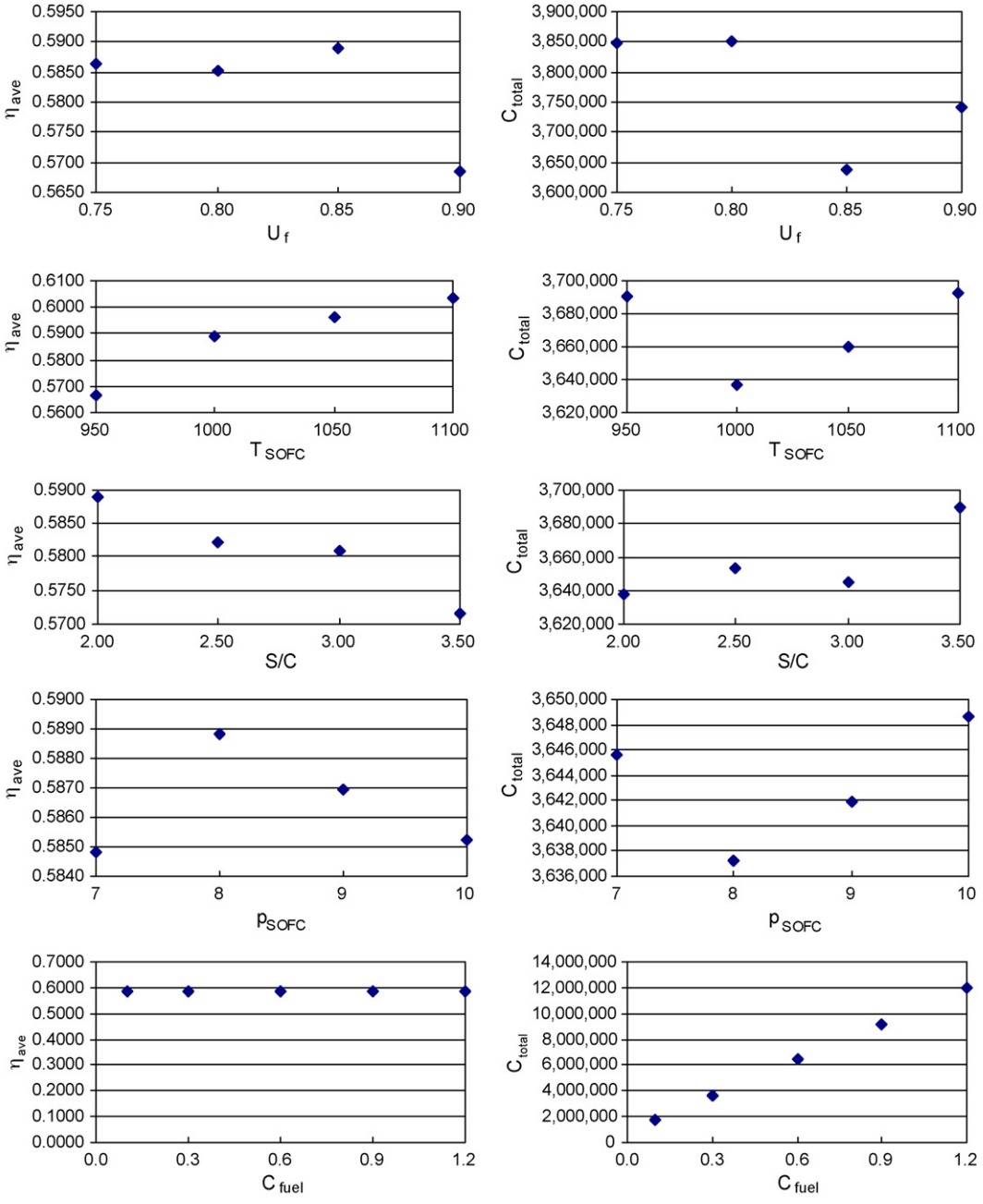

Fig. 2. Optimizing variables vs. objective functions for the 10 MWe triple-pressure w/RH ST small SOFC.

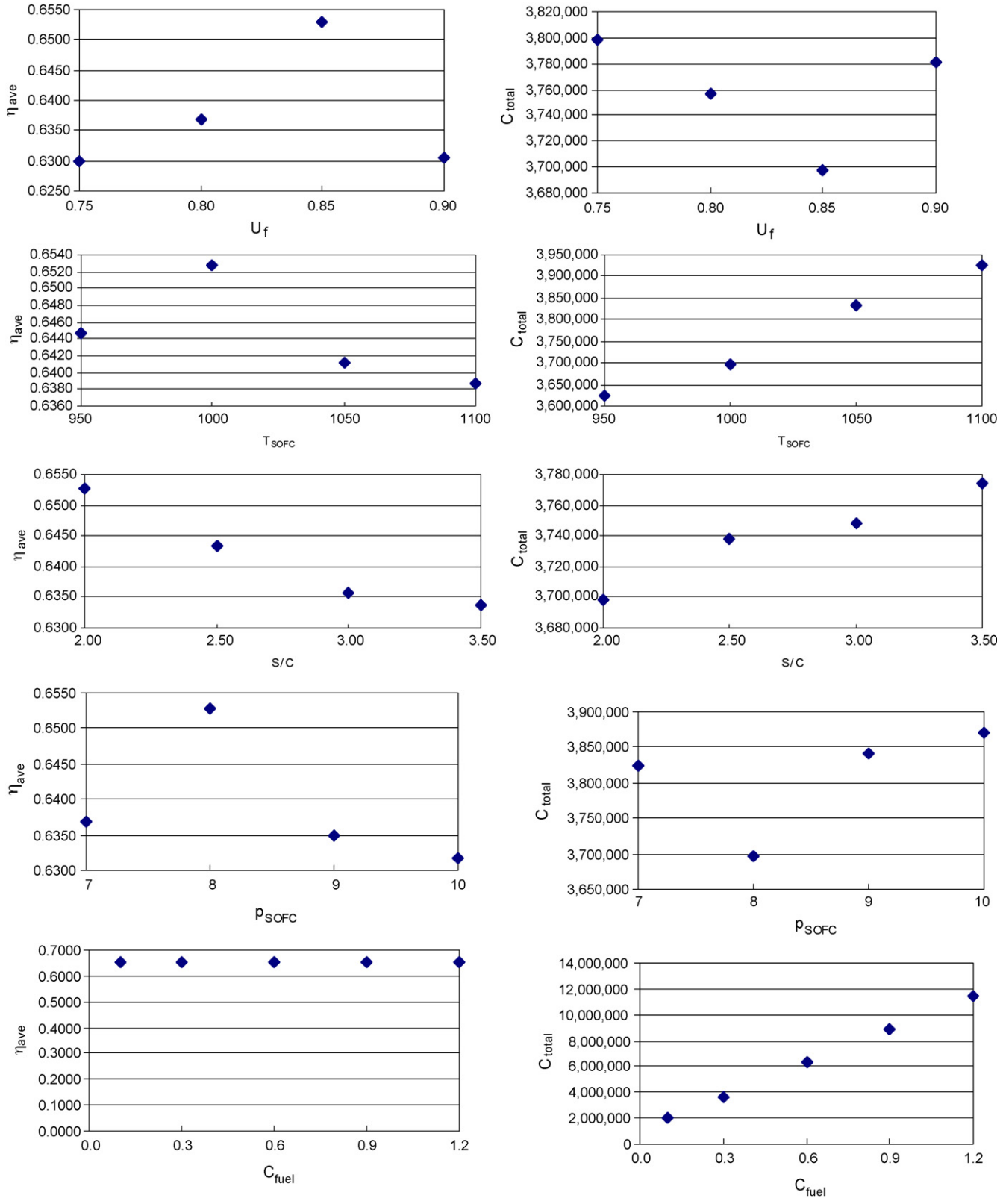

Fig. 3. Optimizing variables vs. objective functions for the 10 MWe triple-pressure w/RH ST large SOFC.

is 0.85 and not 0.90 because at the latter value although the SOFC efficiency is slightly higher, the total plant efficiency drops because not much heat is left for recovery by the gas turbine and the steam turbine since almost all the hydrogen produced by the internal reforming reactions is consumed within the fuel cell by the anode electrochemical reaction and more efficient stacks release less heat. Therefore, the electrical power produced by the SOFC increases, causing a raise in its electro-

chemical rate of reaction. On the other hand, this effect decreases significantly the turbomachinery efficiencies.

The optimum SOFC operating temperature for both SOFC sizes and all models is 1000 °C. For the small SOFC, where the total cost is the optimizing function, the lower the SOFC operating temperature the lower the SOFC capital cost. This trend reaches a minimum at 1000 °C and not 950 °C because the operating cost manages to slightly overcome the capital cost. For the large SOFC, where the average efficiency is the optimizing function, the best SOFC operating temperature is still 1000 °C because although the SOFC stacks operate slightly more efficiently at increased temperatures, the air and fuel compressors require significantly higher power consumption, thereby decreasing slightly the overall efficiency.

The steam-to-carbon ratio reaches its optimum efficiency and lower cost at the lowest possible value of 2. The capital cost remains constant throughout the S/C variation; and, therefore, the only significantly varying cost is the operating cost which will be determined by the overall efficiency. The average efficiency slightly decreases as the S/C increases since higher steam partial pressures cause higher Nernst overvoltages [6]. Thus, higher efficiencies and lower operating/total costs are achieved at lower S/C values.

Theoretically increasing the SOFC operating pressure will result in an increase of the cell voltage because of the higher reactant partial pressure available, therefore, improving the SOFC efficiency. On the other hand, the expansion of the gas in the turbomachinery is in a temperature region where the turbomachinery produces less power as the pressure increases as indicated in [34]. Also, the additional thermal input to the system for delivering air and fuel at the desired conditions leads to a decreasing trend for the overall efficiency when the pressure is increased beyond a certain level. Therefore, the optimum efficiency for both the total cost and efficiency objectives is at an intermediate point (8 bar) where the capital cost is not as high as compared to a capital cost for an even higher pressure where the capital cost of the turbomachinery would increase to accommodate the higher pressure needed. On the other hand, a lower operating pressure causes lower efficiencies and, therefore, although the capital cost is lower the operating cost is higher resulting in an increased total cost.

Finally, the unit cost of fuel variation helps determine how efficiently the overall hybrid plant should be designed. At lower costs of fuel, e.g., 0.1 and 0.3 \$ Nm^{-3}, the capital cost competes more evenly with the operating cost to determine the optimum

Table 5
Optimal component costs for the 10 MWe triple-pressure w/RH ST hybrid system

Component	Cost	
	Large SOFC	Small SOFC
SOFC	5,031,872	2,334,223
GT	1,595,840	1,662,272
Combustor/mixer	1,236,623	941,679
HRSG	584,085	660,761
ST	438,749	536,340
Inlet air tubes	345,616	189,093
AC	258,163	264,960
Deaerator	57,278	67,761
Pre-reformer	45,124	36,994
FC	41,321	42,856
Condenser	8,262	8,262
Pumps	7,958	9,734
Total investment	9,650,891	6,754,935

Table 6
Cost and efficiency breakdown for all optimal models

Configuration	Description	$\dot{W}_{SOFC}$ (MW)	Total cost	Operating cost	Capital cost	η_{ave}	η_{tot}	η_{max}
1	1.5 MWe single-pressure ST small SOFC	1.275	604,743	438,971	165,772	0.5696	0.6022	0.6638
2	1.5 MWe single-pressure ST large SOFC	1.330	613,655	405,328	208,327	0.6235	0.6525	0.6971
3	1.5 MWe dual-pressure ST small SOFC	1.275	602,033	435,146	166,887	0.5705	0.6031	0.6647
4	1.5 MWe dual-pressure ST large SOFC	1.330	611,026	401,575	209,451	0.6243	0.6533	0.6978
5	1.5 MWe triple-pressure ST small SOFC	1.238	599,321	431,428	167,893	0.5712	0.6035	0.6654
6	1.5 MWe triple-pressure ST large SOFC	1.314	608,046	397,831	210,215	0.6251	0.6536	0.6987
7	1.5 MWe triple RH-pressure ST small SOFC	1.234	598,691	430,598	168,093	0.5716	0.6038	0.6657
8	1.5 MWe triple RH-pressure ST large SOFC	1.300	607,446	397,031	210,415	0.6255	0.6539	0.6992
9	5 MWe single-pressure ST small SOFC	4.116	1,887,264	1,437,339	449,925	0.5791	0.6131	0.6795
10	5 MWe single-pressure ST large SOFC	4.333	1,935,053	1,340,421	594,632	0.6264	0.6573	0.7115
11	5 MWe dual-pressure ST small SOFC	4.069	1,872,891	1,411,966	460,925	0.5808	0.6149	0.6815
12	5 MWe dual-pressure ST large SOFC	4.325	1,920,649	1,316,017	604,632	0.6279	0.6589	0.7132
13	5 MWe triple-pressure ST small SOFC	4.054	1,871,891	1,405,966	465,925	0.5814	0.6155	0.6825
14	5 MWe triple-pressure ST large SOFC	4.317	1,924,649	1,310,017	614,632	0.6286	0.6596	0.7142
15	5 MWe triple RH-pressure ST small SOFC	4.037	1,869,891	1,402,966	466,925	0.5817	0.6159	0.6837
16	5 MWe triple RH-pressure ST large SOFC	4.281	1,923,649	1,307,017	616,632	0.6289	0.6601	0.7157
17	10 MWe single-pressure ST small SOFC	7.999	3,630,071	2,831,362	798,710	0.5876	0.6222	0.6922
18	10 MWe single-pressure ST large SOFC	8.495	3,717,621	2,603,916	1,113,705	0.6473	0.6766	0.7272
19	10 MWe dual-pressure ST small SOFC	7.929	3,630,067	2,819,358	810,710	0.5880	0.6228	0.6943
20	10 MWe dual-pressure ST large SOFC	8.485	3,717,624	2,591,919	1,125,705	0.6478	0.6772	0.7292
21	10 MWe triple-pressure ST small SOFC	7.905	3,640,067	2,805,358	834,710	0.5884	0.6234	0.6961
22	10 MWe triple-pressure ST large SOFC	8.474	3,715,624	2,577,919	1,137,705	0.6480	0.6774	0.7292
23	10 MWe triple RH-pressure ST small SOFC	7.958	3,606,144	2,822,572	783,573	0.5891	0.6242	0.6973
24	10 MWe triple RH-pressure ST large SOFC	8.391	3,697,652	2,577,948	1,119,703	0.6529	0.6836	0.7370

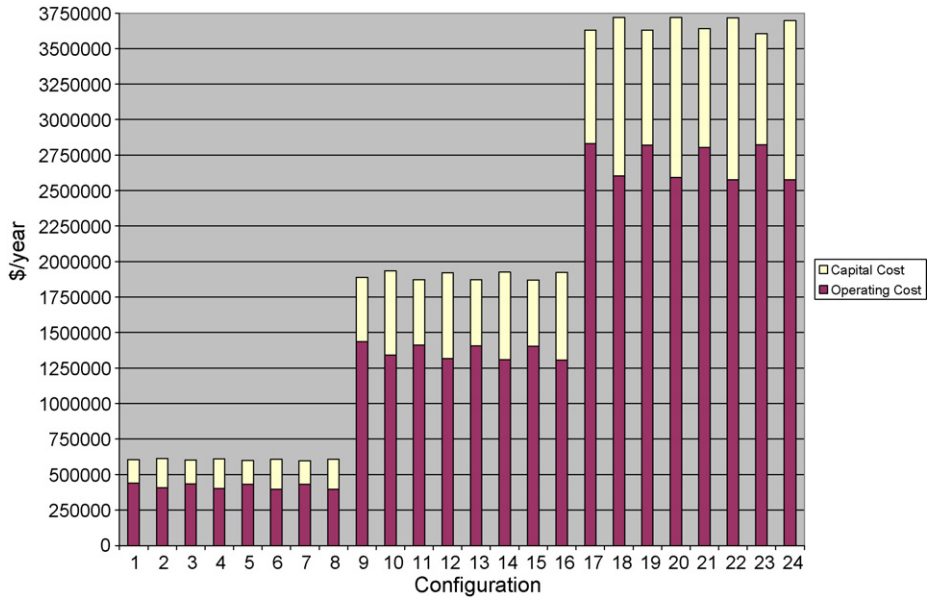

Fig. 4. Cost breakdown for all optimal configurations.

system. On the other hand, at higher values of unit cost of fuel, e.g., 0.9 and 1.2 \$ Nm^{-3}, the operating cost increases far and away above the capital cost and, therefore, a minimization of fuel consumption is required. In such a case, a more efficient system is required, and, therefore, the large SOFC, although having a higher capital cost than the smaller SOFC would be selected.

The component cost breakdown for the 10 MWe triple-pressure reheat ST hybrid system is shown in Table 5. As expected, the most dominant component cost is the SOFC purchase (depreciation) cost (especially when using the large SOFC), while the turbomachinery, combustor, and HRSG costs are also significant.

All twenty-four system configurations are compared in terms of cost (total, operating, and capital) and efficiency (maximum, total, and average) in Table 6. From Fig. 4 it can be concluded that as expected the higher the degree of complexity in the heat recovery steam generator, the higher the capital cost is. On the other hand, the operating cost decreases as this complexity increases because of the increasing efficiency. This decrease in operating cost is significant enough to balance and even slightly decrease the total cost for a more complex system. In terms of SOFC size, the configurations equipped with a smaller SOFC also as expected have a total cost lower than those with the larger SOFC.

Finally, from Fig. 5 it is evident that the efficiency is higher for a system equipped with a larger SOFC than those with a

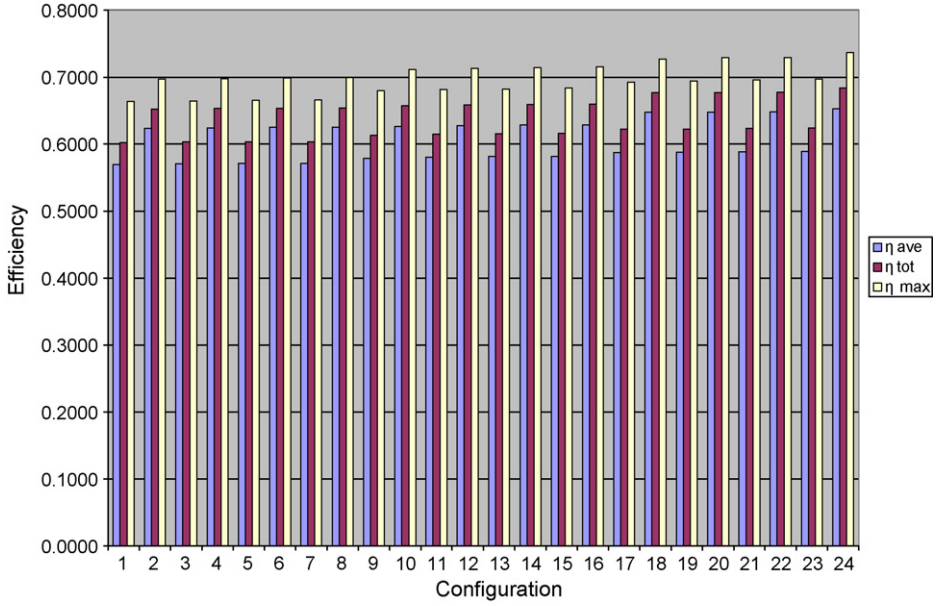

Fig. 5. Efficiency breakdown for all optimal configurations.

smaller SOFC for any given configuration pair. In addition, a global comparison of all twenty-four systems shows that the most efficient system is a system at the larger power capacity level, i.e. the 10 MWe configuration is more efficient than the 5 MWe configuration or the 5 MWe configuration is more efficient than the 1.5 MWe configuration. This is mainly due to the higher efficiencies achieved by the turbomachinery (gas turbine, steam turbine, air compressor, fuel compressor, pumps) at the larger capacities.

7. Conclusions

The high efficiencies developed by some of the hybrid systems are of great interest since they show the potential for exceeding those of the best commercial heat engine cycles currently available or projected. For instance, the 10 MWe SOFC–GT–ST hybrid triple pressure with reheat system exhibits efficiencies (maximum efficiency of 73.8%, an average efficiency of 65.3%, and a total efficiency of 68.4%) that cannot be matched by other conventional and non-conventional cycles (e.g., a standalone SOFC, SOFC–GT hybrid cycles, etc.). Interestingly, the SOFC–GT–ST system develops high efficiencies at off-design conditions as well. However, the off-design strategy followed in this research work was a simplistic one which involved the lowering of the fuel flow rate while keeping constant the air flow rate. This strategy was necessary because a constant air-to-fuel ratio strategy (which maintains high efficiencies) has a very restricted field of operation (above 80% of full load) not applicable for the load profile (down to 25% of full load) considered in this research study. Therefore, this simplistic strategy creates conditions at which, for example, the SOFC operating temperature drops significantly, leading to the difficulty of maintaining higher efficiencies than those actually exhibited. Thus, a more in-depth analysis of the off-design strategy should be done to see if a better strategy can indeed be found (e.g., the removal of part of the SOFC stack at lower loads could conceivably maintain higher efficiencies).

The parametric study identified a number of unforeseen complexities which only became evident after the integration and development of the total system configurations. These difficulties included the proper selection of the SOFC stack size and the difficulty of finding the proper steam turbines to match the system. For a realistic system, a 1.5 MWe SOFC–GT–ST is not as attractive and efficient as a 5 or a 10 MWe system because the gas turbine and especially the steam turbine are very inefficient at small sizes resulting in lower overall system efficiencies.

A careful selection of component designs in the steam turbine cycle was made to achieve efficient conversion of the thermal energy to power output based on the thermodynamic, geometric, and cost models. The uniqueness of the system required in many instances the rescaling and remodeling of existing components to fulfill the needs of the system. Thus, if not careful, one risks making unrealistic selections and cost analyses of equipment. Therefore, the design of a hybrid SOFC–GT–ST power plant must focus on all the components and not only on the SOFC. Special attention must be given in the coupling of the turbomachinery with the SOFC and the heat exchangers in order to achieve the maximum benefits offered by the hybrid system. The air compressor has an unexpectedly high consumption of power (about 75% of the gas turbine power output) meaning that a study must be made in order to minimize this trend if possible. Based on current technology, the SOFC operates at pressures of 7–9 bars meaning that a high degree of compression is required to fulfill this need. New developments in lower temperature and pressure SOFCs may benefit the overall system since less compression will be required.

Since the SOFC–GT–ST system involves a large amount of equipment with a much larger number of decision variables than actually considered in this parametric study, a more complete optimization of the systems should be done in order to determine more detailed syntheses/designs than those presented here.

Finally, since SOFCs are not fully commercialized, a more accurate economic analysis than that made here cannot be made at this time. The high capital cost suggested in this research work (even adjusted for production volume) could decrease in the near future leading to minimized cost syntheses/designs which exhibit even higher efficiencies than those determined here.

References

[1] J. Larminie, A. Dicks, Fuel Cell Systems Explained, John Wiley, Chichester, West Sussex, 2003.
[2] Fuel Cell Handbook, seventh ed., Office of Fossil Energy, National Energy Technology Laboratory, Morgantown, West Virginia, November, 2004.
[3] Siemens Power Generation, http://www.powergeneration.siemens.com, 2007.
[4] F. Calise, Modellazione, Analisi Exergetica ed Ottimizzazione Termoeconomica di Cicli Ibridi SOFC–GT, Università Degli Studi di Napoli Federico II, Napoli, Italy, 2005.
[5] F. Calise, M. Dentice d'Accadia, A. Palombo, L. Vanoli, R. Vanoli, Third International Symposium on Energy and Environment, Sorrento, Italy, 2004.
[6] F. Calise, M. Dentice d'Accadia, L. Vanoli, M.R. von Spakovsky, J. Power Sources 159 (2) (2006) 1169–1185.
[7] S.C. Singhal, K. Kendall, High Temperature Solid Oxide Fuel Cells: Fundamentals, Design, and Applications, Elsevier, Oxford, New York, 2003.
[8] T.G. Benjamin, E.H. Camera, L.G. Marianowski, Handbook of Fuel Cell Performance, Institute of Gas Technology, 1995.
[9] S.H. Chan, C.F. Low, O.L. Ding, J. Power Sources 103 (2) (2002) 188–200.
[10] S. Campanari, Power Plants Based on Solid Oxide Fuel Cells Combined With Gas Turbine Cycles, PhD Dissertation, Politecnico di Milano, Milano, Italy, 1998.
[11] N. Georgopoulos, Application of a Decomposition Strategy to the Optimal Synthesis/Design and Operation of a Fuel Cell Based Total Energy System, M.S. Thesis, advisor: M.R. von Spakovsky, Virginia Polytechnic Institute & State University, Blacksburg, VA, 2002.
[12] B. Oyarzabal, Application of a Decomposition Strategy to the Optimal Synthesis/Design of a Fuel Cell Sub-system, M.S. Thesis, Department of Mechanical Engineering, advisor: M.R. von Spakovsky, Virginia Polytechnic Institute & State University, Blacksburg, VA, 2001.
[13] W.R. Dunbar, N. Lior, R. Gaggioli, Energy: Int. J. 16 (10) (1991) 1259–1274.
[14] S. Campanari, J. Eng. Gas Turbines Power 122 (2) (2000) 239–246.
[15] P. Costamagna, L. Magistri, A. Massardo, J. Power Sources 96 (2) (2001) 352–368.
[16] S. Campanari, J. Power Sources 112 (1) (2002) 273–289.
[17] S. Pelster, Environomic Modeling & Optimization of Advanced Combined Cycle Cogeneration Power Plants Including CO_2 Separation Options, Doc-

toral Thesis, advisors: M.R. von Spakovsky, D. Favrat, Ecole Polytechnique Federale de Lausanne, Lausanne, Switzerland, 1998.
[18] R. Kehlhofer, Combined-Cycle Gas & Steam Turbine Power Plants, PennWell Pub. Co., Tulsa, Oklahoma, 1999.
[19] S. Kakaç, H. Liu, Heat Exchangers: Selection, Rating, and Thermal Design, second ed., CRC Press, Boca Raton, Florida, 2002.
[20] A. Arsalis, Thermoeconomic Modeling and Parametric Study of Hybrid Solid Oxide Fuel Cell-Gas Turbine-Steam Turbine Power Plants Ranging from 1.5 MWe to 10 MWe, M.S. Thesis, advisor: M.R. von Spakovsky, Virginia Polytechnic Institute and State University, Blacksburg, VA, 2007.
[21] J.K. Salisbury, Steam Turbines and Their Cycles, R.E. Krieger Publication Company, Huntington, New York, 1974.
[22] B.G.A. Skrotzki, W.A. Vopat, Power Station Engineering and Economy, McGraw-Hill, New York, 1960.
[23] P.J. Potter, Power Plant Theory and Design, Ronald Press Co., New York, 1959.
[24] A. Traverso, A. Massardo, W. Cazzola, G. Lagorio, ASME Paper 2004-GT-54115, 14–17 June, 2004, Proceedings of ASME-IGTI TURBO EXPO 2004, Vienna, Austria, 2004.
[25] P. Chiesa, S. Consonni, Second Annual Conference on Carbon Sequestration, Washington, DC, USA, 2003.
[26] R.F. Boehm, Design Analysis of Thermal Systems, John Wiley and Sons, Inc., New York, 1987.
[27] Chemical Engineering Plant Cost Index, Chemical Engineering, McGraw-Hill, New York, 2006.
[28] A. Traverso, Personal Communication on the Purchase Cost Function of Condensing, Axial Type Steam Turbines, Virginia Tech, Blacksburg, Virginia, 2006.
[29] C.A. Frangopoulos, Int. J. Energy Environ. Econ. 1 (4) (1991) 275–287.
[30] M.S. Peters, K.D. Timmerhaus, R.E. West, Plant Design and Economics for Chemical Engineers, McGraw-Hill, New York, 2003.
[31] Energy Information Administration, U.S. Natural Gas Prices, http://www.eia.doe.gov, 2006.
[32] S.C. Singhal, Fifth International Symposium on SOFC, Aachen, Germany, July 2–5, 1997.
[33] D. Rancruel, Optimization of Solid-Oxide Fuel Cell Balance-of-Plant System, PhD Dissertation, advisor: M.R. von Spakovsky, Virginia Polytechnic Institute & State University, Blacksburg, VA, 2005.
[34] T.P. Chen, J.D. Wright, K. Krist, NETL Proceedings of the Fuel Cells '97 Review Meeting, GRI study, 1997.